Ripening of monolayer vacancy pits on metal surfaces: Pathways, energetics, and size-scaling for Ag(111) versus Ag(100)

Mingmin Shen, J.-M. Wen,* C. J. Jenks, and P. A. Thiel
Department of Chemistry and Ames Laboratory, U.S. DOE, Iowa State University, Ames, Iowa 50011, USA

Da-Jiang Liu
Ames Laboratory, U.S. DOE, Iowa State University, Ames, Iowa 50011, USA

J. W. Evans
Department of Mathematics and Ames Laboratory, U.S. DOE, Iowa State University, Ames, Iowa 50011, USA
(Received 13 July 2006; revised manuscript received 22 March 2007; published 7 June 2007)

Scanning tunneling microscopy studies have revealed that monolayer-deep vacancy pits typically coarsen at 300 K via Smoluchowski ripening (SR) on Ag(111) surfaces and via Ostwald ripening (OR) on Ag(100) surfaces. We elucidate the underlying atomistic processes, the relevant energetics with some input from density functional theory analysis, and also the scaling of the ripening rate with mean pit size. Size scaling for SR reflects the size dependence of the pit diffusion coefficient, so we also discuss observed deviations from classical theories. SR dominates OR for pits on Ag(111) primarily due to its significantly lower effective energy barrier. However, the effective barrier for OR is not lower than that for SR for pits on Ag(100), and one must also account for the distinct size scaling of these pathways to explain the dominance of OR. We also briefly discuss the dependence on temperature of the dominant ripening pathway and the ripening behavior for adatom islands.

DOI: 10.1103/PhysRevB.75.245409 PACS number(s): 68.35.Fx, 68.55.Jk, 68.37.Ef, 68.47.De

I. INTRODUCTION

Coarsening or ripening phenomena are ubiquitous for two-phase materials from solid alloys to surface deposits to liquid droplets.[1] The driving force for evolution is reduction of the excess free energy associated with the interface regions between the two phases. The most common mechanism for coarsening of convex domains or aggregates of a minority phase embedded in a majority phase is Ostwald ripening. This mechanism involves mass transfer between smaller and larger aggregates, leading to growth of the latter. This is a curvature-driven process reflecting the higher chemical potential of smaller aggregates.

One class of two-phase systems with an embedded minority phase is provided by single-atom-high islands for adlayers with lower precoalescence coverages on low-index single-crystal metal surfaces. These island distributions are typically formed by deposition of up to roughly 0.3 monolayers and are embedded in a very dilute two-dimensional gas phase of adatoms. Another class is provided by single-atom-deep vacancy pits embedded in the surrounding terrace. Such distributions of pits can be formed either by sputtering of the surface or by depositing adlayers with higher near-monolayer coverages as described below. These classes of systems are ideally suited for fundamental studies of coarsening phenomena in two-dimensions.[2–4] In this paper, we focus on analysis of the latter, vacancy pit ripening, for Ag single-crystal surfaces.

Previous experimental studies have revealed a stark contrast in the ripening mechanism observed for monolayer-deep vacancy pits on the (111) and (100) faces of an Ag single-crystal substrate at 300 K. Smoluchowski ripening (SR)—i.e., vacancy pit diffusion and coalescence—occurs for pits on Ag(111).[2,5] In contrast, Ostwald ripening (OR)—i.e., dissolution of smaller pits and associated growth of larger pits—occurs for pits on Ag(100).[6] The corresponding difference in ripening pathways is also observed at 300 K if the substrate is Cu rather than Ag.[3] In this paper, we will determine the origin of this differing behavior for Ag(111) versus Ag(100) by examining the following factors.

(i) *Possible underlying atomistic mass transport processes contributing to ripening*. We emphasize that the mass transport underlying OR could potentially be dominated by terrace diffusion of either adatoms or isolated vacancies. For SR in the systems of interest here, it is commonly accepted that periphery diffusion of adatoms along the step edges bounding pits is the dominant factor in pit diffusion. See Fig. 1 for a schematic of these atomistic processes.

(ii) *Overall or effective barriers E_{eff} for these ripening pathways*. We shall decompose these effective barriers into their various components, and determine these either from utilization of previous experimental data or from previous or new density functional theory calculations.

(iii) *Scaling of the ripening rate with mean pit size*. This basic behavior can be formulated in terms of simple generic equations which have essentially the same for form either of the above mentioned OR or SR ripening mechanisms. See the discussion immediately below.

For our formulation of size scaling, we let $L_{av}=L_{av}(t)$ denote the mean linear size or "diameter" of vacancy pits at time t, where L_0 gives the initial value. These quantities, as well as other lengths introduced below, are measured in dimensionless units of the surface lattice constant a. Then, we identify $K=dL_{av}/dt$ as the coarsening or ripening rate. For either OR or SR, the key quantities L_{av} and K satisfy the scaling forms[4,7]

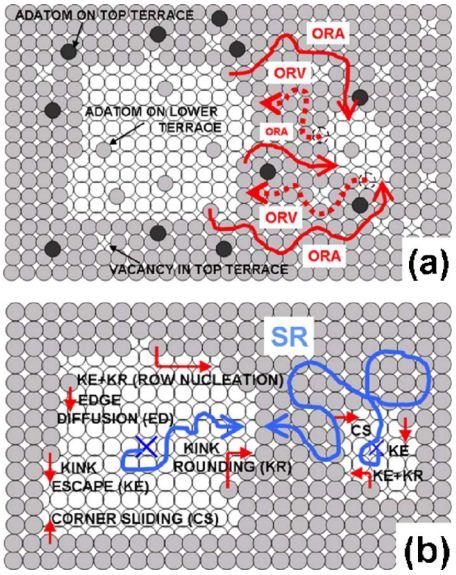

FIG. 1. (Color online) Schematics for atomistic processes underlying ripening of vacancy pits for an fcc(100) crystal geometry. Gray atoms represent the top surface layer. White atoms represent the underlying layer exposed within the monolayer pits. (a) Possible mass transport pathways operative in OR involving single adatoms (ORA) and single vacancies (ORV) diffusing between different-sized vacancy pits. There are higher concentrations of isolated adatoms around the larger pit and of isolated ad-vacancies around the smaller pit. Black adatoms are diffusing on top of the gray surface layer. (b) Periphery-diffusion processes underlying diffusion of vacancy pits. We indicate nucleation of a new empty row on the top edge of the left pit (by removal of an adatom adjacent to an isolated vacancy). We also indicate the dominant process leading to formation of an isolated vacancy on the lower edge—i.e., corner sliding. See Sec. IV for related discussion. The overall motion of the center of masses (indicated by $\times$) of the pits, potentially leading to coalescence, is also shown by a meandering path.

$$L_{\mathrm{av}}(t) \approx L_0(1 + t/\tau)^n \tag{1}$$

with characteristic time

$$\tau = \tau_0 \exp[E_{\mathrm{eff}}/(k_B T)]$$

and, correspondingly,

$$K \approx \nu \exp[-E_{\mathrm{eff}}/(k_B T)](L_{\mathrm{av}})^{-m} \tag{2}$$

with

$$m = n^{-1} - 1$$

and

$$\nu = (L_0)^{1/n} n/\tau_0.$$

Here, E_{eff} denotes the effective or overall activation barrier for the ripening process, T denotes the surface temperature, and k_B is the Boltzmann constant. Often temporal scaling behavior for ripening is formulated in terms of the average center-to-center pit separation $L_{\mathrm{isl}} \sim \varphi^{-1/2} L_{\mathrm{av}}$, where φ denotes the areal coverage of the pits. Since φ is constant during ripening, L_{isl} and L_{av} exhibit the same temporal scaling.

For OR, one has that $n=1/3$ (so $m=2$) in the regime where mass transport is limited by terrace diffusion,[4] and $n=1/2$ (so $m=1$) in the regime of attachment-detachment-limited mass transport.[4] For the attachment-detachment-limited OR, there exists a significant additional barrier inhibiting attachment to pits (See Appendix A). For SR, we assume that the diffusion coefficient for vacancy pits of "large" linear size L scales like[8]

$$D_{\mathrm{pit}}(L) \approx D_0 \exp[-E_{\mathrm{eff}}/(k_B T)] L^{-\beta}, \tag{3}$$

where E_{eff} will also correspond to the effective energy for ripening in (1) and (2). Then, a simple Smoluchowski-type rate equation analysis of ripening kinetics reveals that the scaling forms (1) and (2) apply with $n=1/(2+\beta)$ (so $m=1+\beta$) [7,9] (See again Appendix A). Clearly, a comprehensive analysis of the ripening rates for competing pathways includes both determination of the relevant energetics and assessment of size scaling. This type of analysis seems to be lacking in the existing literature, but we shall see that it is needed to explain the experimentally observed behavior for vacancy pit ripening on Ag surfaces.

In Sec. II, we briefly review experimental observations on ripening of vacancy pits on Ag surfaces. Then, a description underlying atomistic processes and a detailed analysis of the energetics for OR of vacancy pits on Ag surfaces follows in Sec. III. Next, a description of the atomistic processes and an analysis of the energetics for SR of vacancy pits on these surfaces is provided in Sec. IV. A comparison of ripening rates for OR and SR incorporating appropriate size-scaling behavior is provided in Sec. V. Finally, conclusions are provided in Sec. VI, as well as a brief discussion of analogous issues for ripening of adatom islands.

II. REVIEW OF EXPERIMENTAL OBSERVATIONS

Procedures for our own sample preparation can be found in Ref. 10 for Ag(100) and in Ref. 11 for Ag(111). Extensive previous data for vacancy pit ripening on Ag(111) are available from studies of Morgenstern and co-workers, and their sample preparation procedures are described in Refs. 2, 5, and 12–14. All observations of pit ripening where made utilizing scanning tunneling microscopy on single-crystal surfaces with broad terraces under ultrahigh-vacuum conditions.

Vacancy pit ripening and diffusion behavior for Ag(111). As indicated in Sec. I, distributions of pits are conveniently formed by sputtering of large terraces on an Ag(111) surface. Previous studies[2,5] of large arrays of vacancy pits on Ag(111) at 300 K have revealed that evolution is dominated by SR. For pits with diameters in the range $L_0 \sim 15-60$, a significant reduction in the pit density occurs on the time scale of ~ 1 h at 300 K. Our own studies also find this behavior. No island dissolution is observed, although this cannot be ruled out for some of the smallest islands, so that coarsening occurs either primarily or exclusively by SR. In new studies, we have observed similar SR of smaller ensembles of vacancy pits confined on a finite terrace surrounded mainly by ascending steps, so that pit ripening behavior is isolated from the higher terraces by the presence of a step-edge barrier (see below). However, one edge of this terrace was bounded by a de-

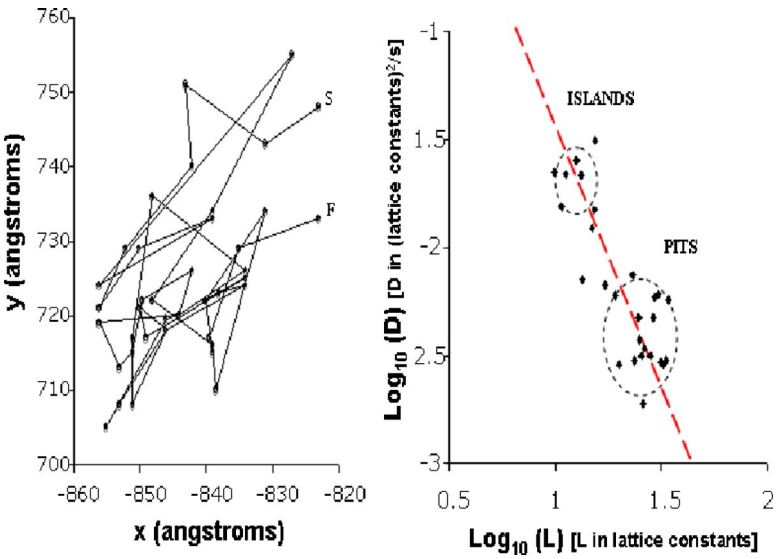

FIG. 2. (Color online) (a) Center-of-mass motion at 300 K for a vacancy pit on Ag(100) with 950 missing atoms (S, starting position; F, final position after ~500 min); (b) log D-log L plot showing diffusion coefficients D for set of 18 pits with $L=25\pm15$ (grouped within large dashed circle) *plus* D for set of 9 islands with $L=13\pm5$ (grouped within small dashed circle). Dashed line through the centers of these dashed circles has a slope of about −2.3 corresponding to the size scaling exponent determined in Ref. 15 for adatom islands. The D values in Ref. 15 are systematically lower than here, perhaps reflecting a slightly lower T in those studies or perhaps strain effects due to the higher island density.

scending step, and we observe that as the tip scans across this descending terrace from the lower to the upper terrace of interest, occasionally small pits are formed due to a tip effect. Subsequently, these disappeared relatively quickly due to coalescence.

Previous studies have also provided a detailed analysis of the diffusivity of these monolayer vacancy pits. The initial study of pit diffusion at 300 K found a size-scaling exponent of $\beta\approx2.0$—i.e., $D_{\text{pit}}(L)\sim L^{-2}$.[12] A subsequent study examining behavior for various T revised the estimate of this exponent to $\beta\approx1.5$ at 300 K (although statistics were more limited), and it was observed that β tends to increase with T.[13] This later study also extracted an effective barrier varying from $E_{eff}\approx0.6$ eV for smaller $L\approx13$ to $E_{eff}\approx0.5$ eV for larger $L\approx80$.[13] We will both utilize and elucidate these results in Secs. IV and V.

Another significant observation comes from previous studies,[14] and also our own experiments, where an adatom island exists in the immediate vicinity of one or more vacancy pits. This island is observed to dissolve with its area decaying nonlinearly in time as is indicative of diffusion-limited decay.[2,3] See Appendix A. However, essentially none of its atoms fill the neighboring vacancy pits, but rather attach to more distant ascending steps. This feature provides direct support for the commonly recognized existence of a large Ehrlich-Schwoebel step-edge barrier δ_{ES} (in excess of the terrace diffusion barrier), which strongly inhibits downward transport of adatoms in the Ag/Ag(111) system.[2]

Vacancy pit ripening and diffusion behavior for Ag(100). In these studies, distributions of pits were created as follows. Deposition of 0.8–0.9 monolayers at 300 K produced adlayer morphologies with an incomplete first layer containing irregular vacancy clusters formed due to coalescence and percolation of adatom islands. There was also a low population of second layer islands. A short time after deposition (with the temperature maintained at 300 K), the second layer atoms were incorporated into the first layer and the irregular vacancy clusters restructured to form an array of separated near-square vacancy pits.

Analysis of the evolution of arrays of dozens of vacancy pits with size $L_0\sim20-60$ on a large terrace at 300 K reveals noticeable coarsening over a period of 6 h almost exclusively due to OR. While ripening was dominated by OR, we emphasize that the vacancy pits were not completely immobile during the ripening process. In fact, significant pit diffusion was observed. One can track the motion of the center of mass of individual pits for a period of time over which their size does not vary significantly. See Fig. 2(a). In this way, we are able to estimate the diffusion coefficients $D_{\text{pit}}(L)$, for pits of various linear sizes L. We have determined D_{pit} for 18 vacancy pits on Ag(100) with linear dimensions in the range $L\approx25\pm10$. These data, which reveal an average diffusion coefficient of $D_{\text{pit}}(L\approx25)\approx3.5\times10^{-3}$ a^2/s, are shown in Fig. 2(b).

In the following analysis, we will propose that large vacancy pits and adatom islands on Ag(100) with the same size have roughly equal diffusion coefficients. See also Sec. V. This is generically true in the "continuum regime" of very large sizes $L\gg L_c$, where $L_c\approx70$ at 300 K is the mean separation between kinks on a close-packed step edge (see below). In this regime, the size-scaling exponent for cluster diffusion mediated by periphery diffusion satisfies $\beta=3$.[8] However, we will also claim that this rough equality of island and pit diffusion coefficients applies for the regime of smaller sizes $L\approx10-35$. Here, the size-scaling exponent $\beta\approx2.3$ has been shown to deviate significantly below the continuum value for adatom islands.[15] Thus, by our assumption, $\beta\approx2.3$ for vacancy pits in this size range. Experimental support for our proposal is provided in Fig. 2(b), where we also show a subset of our previous data[10] for diffusion coefficients D_{isl} of nine adatom islands with a range of smaller linear sizes $L\approx13\pm5$ yielding an average value of $D_{\text{isl}}(L\approx13)\approx1.5\times10^{-2}$ a^2/s. Our data for adatom islands or vacancy pits separately are not extensive enough to assess size scaling. However, together the data are consistent with our proposal for similar diffusion coefficients of islands and pits with a common size scaling exponent of $\beta\approx2.3$. (Note that Ref. 6 made the misleading assertion that the diffusion coefficient for vacancy pits is smaller than that for adatom islands. This assertion was based on a neglect of the decrease of diffusion coefficient with pit or island size.)

III. ENERGETICS FOR OSTWALD RIPENING OF VACANCY PITS

Traditionally, ripening in submonolayer metal homoepitaxial systems has invariably been expected to occur via the OR pathway.[4] Thus, we first analyze the associated OR energetics for vacancy pits. These results are summarized again in Sec. V. We thereby provide insight into why OR is inefficient for vacancy pits on Ag(111), but more efficient on Ag(100). As indicated in Sec. I, there are potentially two mass transport pathways which could contribute to OR in these systems [see Fig. 1(a)].

(i) *Adatom transport* (ORA) where the overall effect is that single adatoms detach from the edges of larger pits, climb up onto and diffuse across the surrounding terrace, and then descend into the smaller pits attaching to their edges.

(ii) *Vacancy transport* (ORV) where the overall effect is that single vacancies detach from the edges of smaller pits, then diffuse across the terrace and attach to the edges of larger pits (a process involving only intralayer hopping of atoms).

For ORA, one can apply the Gibbs-Thomson relation[4] to determine the equilibrium density (per site) ρ_{ad} of single adatoms on the upper or lower terraces immediately adjacent to the edge of a pit. If R denotes the local "pedal" radius[16] of the pit and $\gamma>0$ denotes the local step energy per atom, then one has that

$$\rho_{\mathrm{ad}}(R) = \rho_0 \exp[-\gamma/(k_B T R)], \text{ where } \rho_0 \sim \exp[-E_b/(k_B T)]. \tag{4}$$

Here, ρ_0 gives the equilibrium density adjacent to a straight step and $E_b>0$ denotes the effective detachment energy from such a step.[4,16] The ratio γ/R is constant along the step edge for equilibrated pit shapes,[16] and often one interprets γ as a mean step energy and R as a mean radius. Thus, adatoms diffuse from regions of higher density surrounding larger pits to those of lower density around smaller pits. Since such atoms must surmount the additional Ehrlich-Schwoebel step-edge barrier δ_{ES} in both climbing out of and descending into pits, the effective barrier for this ripening pathway is given by $E_{\mathrm{eff}}(\mathrm{ORA})=E_d(\mathrm{ad})+E_b+\delta_{\mathrm{ES}}$, where $E_d(\mathrm{ad})$ is the adatom terrace diffusion barrier. More precisely, this result applies for significant step-edge barriers (the case of relevance here) where the associated characteristic Ehrlich-Schwoebel length $L_{\mathrm{ES}}=\exp[\delta_{\mathrm{ES}}/(k_B T)]-1$, far exceeds pit separations.

For ORV, the equilibrium density of single vacancies surrounding a pit of radius R has the Gibbs-Thomson form[4]

$$\rho_{\mathrm{vac}}(R) = \rho_0 \exp[+\gamma/(k_B T R)], \text{with } \rho_0 \text{ and } E_b \text{ as above} \tag{5}$$

(for pairwise adspecies interactions). Thus, single vacancies diffuse from regions of higher density around smaller pits to those of lower density around larger pits. Since no step-edge barrier need be surmounted for this intralayer process, the effective barrier for this ripening pathway is $E_{\mathrm{eff}}(\mathrm{ORV})=E_d(\mathrm{vac})+E_b$, where $E_d(\mathrm{vac})$ is the vacancy terrace diffusion barrier.

Absence of OR for vacancy pits on Ag(111). First, consider the ORA pathway on Ag(111). The value of the adatom terrace diffusion barrier of $E_d(\mathrm{ad})=0.10$ eV is well established from both theory and experiment.[17] Appendix B gives our consistent estimate from density functional theory (DFT) analysis. If ϕ denotes the nearest-neighbor (NN) bond energy for a pair of Ag adatoms on the Ag(111) surface, then the detachment energy on fcc(111) surfaces satisfies $E_b=3\phi$, noting that three bonds are broken when an atom detaches from a kink site along a step edge. A previous DFT study using a 4×4 supercell reported a somewhat high value of $\phi=0.24$ eV.[18] However, our own DFT analysis reveals a surprisingly slow convergence with increasing lateral supercell size to the more precise value of $\phi=0.19$ eV for a 6×6 supercell. See Appendix B. If one uses the commonly adopted value for the "large" step-edge barrier of $\delta_{\mathrm{ES}} \approx 0.13$ eV,[2] then one obtains for the OR pathway mediated by adatom transport a value of $E_{\mathrm{eff}}(\mathrm{ORA}) \approx 0.8$ eV. In Sec. IV, we shall see that this is significantly higher than the effective barrier for SR, indicating that this ORA pathway may be inactive.

Second, consider the ORV pathway. While this pathway has the advantage that no step-edge barrier need be surmounted, a critical factor is the efficiency of vacancy diffusion. To assess this factor, we have performed DFT calculations to determine the terrace diffusion barrier for single vacancies. We find that $E_d(\mathrm{vac})=0.58$ eV for a 3×3 supercell which is reasonably consistent with a previous estimate using semiempirical potentials.[19] See Appendix B. This high value should be expected since vacancy diffusion occurs via hopping of an adjacent atom into an isolated vacancy and its motion is highly constrained. Thus, one obtains for the OR pathway mediated by vacancies an even larger value of $E_{\mathrm{eff}}(\mathrm{ORV})=E_d(\mathrm{vac})+3\phi>1.1$ eV which will be shown to be far too high for ORV to be operative.

OR for vacancy pits on Ag(100). First, consider the ORA pathway on Ag(100). The adatom terrace diffusion barrier has the value $E_d(\mathrm{ad})=0.40-0.45$ eV from theory and experiment.[17,20] See Appendix B for our own consistent DFT estimate. Also, it is known from analysis of experimental studies of kinetic roughening during multilayer growth that a step-edge barrier exists only along close-packed edges with a low value of $\delta_{\mathrm{ES}}=0.07$ eV.[17,20,21] The detachment energy satisfies $E_b=2\phi$ on fcc(100) surfaces for NN adatom bond energy ϕ, noting that two bonds are broken upon detaching an adatom from a kink site. A previous DFT estimate gave $\phi=0.22$ eV,[22] which is slightly above our own estimates. See Appendix B. Thus, we conclude that the effective barrier for OR by adatom transport is $E_{\mathrm{eff}}(\mathrm{ORA}) \approx 0.9$ eV.

Second, the ORV pathway again has the advantage that no ES barrier need be surmounted, although that would not be a major impediment for Ag(100). However, another significant factor is suggested by previously available semiempirical analyses of energetics.[19,23] These indicate that the activation barrier for single vacancy diffusion is generally comparable to or even somewhat lower than for adatom diffusion on metal (100) surfaces. This contrasts behavior on metal (111) surfaces. Roughly speaking, vacancy diffusion involves adatom motion reminiscent of escape from a kink along a step edge for which the barrier is the sum of a low step diffusion barrier and the NN interaction ϕ. For a more precise analy-

sis, we apply DFT to obtain $E_d(\mathrm{vac})=0.35$ eV for the Ag(100) surface from a 3×3 supercell. See Appendix B. Thus, the effective barrier for OR by vacancy diffusion is $E_{\mathrm{eff}}(\mathrm{ORV})\approx0.8$ eV. This value is lower than $E_{\mathrm{eff}}(\mathrm{ORA})$, indicating that vacancy transport should dominate adatom transport pathway in the observed OR process. It remains to explain why this pathway is more efficient than SR which we shall see in Sec. IV has a lower effective barrier.

IV. ENERGETICS AND SIZE-SCALING FOR SMOLUCHOWSKI RIPENING OF VACANCY PITS

As indicated in Sec. I, the ripening rate for SR and its scaling with mean vacancy pit size is determined by the diffusion coefficient for the large pits and the scaling of this diffusion coefficient with pit size. For Ag(100) and Ag(111) surfaces, pit or island diffusion is believed to be mediated by *periphery diffusion* of adatoms along step edges.[2,5,15,24–27] We now discuss the corresponding energetics. Results are also summarized in Sec. V. The traditional *continuum treatment* of cluster diffusion mediated by periphery diffusion predicts a diffusion coefficient of the form (3) with scaling exponent $\beta=3$.[2,8] This diffusion coefficient is also proportional to the product of the adatom step-edge mobility, $\sigma_e\sim\exp[-E_{\mathrm{mob}}/(k_BT)]$, and the density of adatom carriers, $\rho_{\mathrm{edge}}\sim\exp[-\phi/(k_BT)]$, for mass transport along the step edge. The effective energy for the mobility satisfies $E_{\mathrm{mob}}=E_e+\delta_{\mathrm{KES}}$, where E_e is the barrier for diffusion of adatoms along straight close-packed steps and δ_{KES} is the additional kink rounding barrier (sometimes referred to as the kink Ehrlich-Schwoebel barrier); ϕ is the NN pair interaction as above. Thus, the effective activation energy for cluster diffusion and for ripening in this treatment satisfies $E_{\mathrm{eff}}(\mathrm{SR})=E_{\mathrm{mob}}+\phi=E_e+\phi+\delta_{\mathrm{KES}}$ (continuum). The carriers are identified as edge adatoms since isolated edge vacancies have a higher barrier for diffusion along straight steps.

However, as noted in Sec. III, deviations from classic continuum scaling with $\beta<3$ are often observed.[13,15] To understand this behavior, one can utilize *atomistic models* for periphery diffusion which provide a realistic treatment of the numerous distinct types of adatom hops and barriers for edge diffusion associated with different local step configurations. Such models exclude detachment, but satisfy detailed balance for all allowed edge hops. Most such studies have focused on adatom island diffusion rather than vacancy pit diffusion. However, the key concepts deriving from the former studies should apply for vacancy pits. It is convenient to introduce a characteristic length corresponding to the typical separation between kinks on equilibrated close-packed step edges, $L_c\approx\exp[\varepsilon_{\mathrm{kink}}/(k_BT)]$, where $\varepsilon_{\mathrm{kink}}\approx\phi/2$ is the kink creation energy. Since $\varepsilon_{\mathrm{kink}}\approx0.11$ eV for an Ag(100) surface,[3] consistent with our use of $\phi\approx0.22$ eV, one has that $L_c\approx70$ at 300 K as mentioned above. For Ag(111), $\varepsilon_{\mathrm{kink}}\approx0.10$ eV (Ref. 4) and $L_c\approx50$ at 300 K are slightly smaller. In general terms, the primary component of the deviation from continuum scaling occurs for L smaller than L_c due to faceting of the vacancy pit (or adatom island) shapes. Another secondary component occurs with significant kink rounding barriers for L smaller than the so-called kink Ehrlich-Schwoebel length $L_{\mathrm{KES}}=\exp[\delta_{\mathrm{KES}}/(k_BT)]-1$.

More specifically, these deviations from classic behavior associated with *faceted clusters* reflect the difficulty to nucleate a new outer vacant row (or filled row) of sites on an otherwise perfect close-packed pit (or island) step edge.[27–29] This process is a necessary component of long-range cluster diffusion. If new outer rows are not created, the cluster can never move outside of a rectangle inscribing it for an Ag(100) surface or a hexagon inscribing it for an Ag(111) surface. We now analyze the associated energetics for periphery diffusion models with no detachment and thus no background equilibrium density of isolated vacancies (adatoms) on the terrace surrounding the pit (island). For *adatom islands*, the density of isolated adatoms on a perfect close-packed step, $\rho_{\mathrm{edge}}\sim\exp[-\phi/(k_BT)]$, is low as these atoms would rather be incorporated at kink sites elsewhere on the island periphery. To nucleate a new outer filled row on this edge, another adatom must detach from a kink site on another edge and round a corner (with effective barrier of $\sim E_e+\phi+\delta_{\mathrm{KES}}$) in order to aggregate with this lone atom before it is re-incorporated at a kink. Thus, accounting for the T dependence of ρ_{edge}, one obtains a total effective barrier of $E_{\mathrm{eff}}(\mathrm{SR})\approx E_e+2\phi+\delta_{\mathrm{KES}}$ (faceted).[27] For *vacancy pits*, the picture is analogous. The density of isolated vacancies on a perfect close-packed step edge is again $\rho_{\mathrm{edge}}\sim\exp[-\phi/(k_BT)]$. To nucleate a new outer vacant row on this edge, an atom adjacent to this vacancy could be transported away to a distant kink site (with effective barrier $E_e+\phi+\delta_{\mathrm{KES}}$). See the top portion of the schematic Fig. 1(b) which illustrates this process. This again leads to the result that $E_{\mathrm{eff}}(\mathrm{SR})\approx E_e+2\phi+\delta_{\mathrm{KES}}$ (faceted).

To create isolated vacancies on a perfect outer step edge of a vacancy pit within these periphery diffusion models, it is necessary for a highly coordinated atom to be extracted from a straight step edge—i.e., to extract a triply coordinated atom for Ag(100) and a quaduply coordinated atom for Ag(111). In contrast for adatom islands, it is not necessary to extract any highly coordinated adatoms from step edges in order to achieve nucleation of new rows and thereby long-range island diffusion. Returning to consideration of vacancy pits, it should be noted that the effective barrier for extraction of a highly coordinated atoms from some central portion of a straight step edge is in fact equal to $E_{\mathrm{eff}}(\mathrm{SR})$. (This is most easily seen by noting that the reverse process corresponds to corner or kink rounding with a barrier of $E_e+\delta_{\mathrm{KES}}$. Thus, using detailed balance, the barrier for extraction equals this value plus the energy difference of 2ϕ between initial and final configurations.) However, again using detailed-balance arguments, one might anticipate that the effective barrier for sliding an atom out of a highly coordinated corner site of the pit and along a step edge equals the lower value of $E_e+2\phi$. This is confirmed by analysis using semiempirical potentials for Ag(100), where the kink rounding barrier is significant.[23] Thus, for pits on Ag(100), one expects that most isolated vacancies on outer edges are created by this "corner-sliding" process. See the lower left portion of the schematic Fig. 1(b) which illustrates this process.

The above discussion does not address deviations from continuum size scaling as this requires a more detailed analy-

TABLE I. Summary of our estimates for the values of key energies (in eV) for Ag(111) and Ag(100) surfaces. Uncertainties are indicated in the text. Also shown are effective energies for OR of vacancy pits via adatom transport (ORA) and via vacancy transport (ORV), and for SR of vacancy pits where pit diffusion is mediated by periphery diffusion. The SR energy is estimated from continuum theory. Values used for the analysis in Sec. V are slightly modified (see the text) or rounded off.

	ϕ	E_d(ad)	E_d(vac)	δ_{ES}	E_e	δ_{KES}	E_{eff}(ORA)	E_{eff}(ORV)	E_{eff}(SR)
Ag(111)	0.19	0.10	0.58	0.13	0.30	0.05	0.80	1.15	0.54
Ag(100)	0.21	0.43	0.35	0.07	0.25	0.16	0.92	0.77	0.62

sis. See Refs. 27 and 28 for a more complete discussion. Here, we just summarize the results. In the regime of strongly facetted islands or pits, one has that $\beta \to 1$ for $\delta_{KES}=0$. For the case of significant kink rounding barriers with L below L_{KES}, one finds even lower values of β at least for adatom islands.[27] In practice, observed behavior is often in the crossover regime between the continuum and completely facetted limits. Thus, the effective β is expected to decrease with decreasing T (or L), and the effective energy E_{eff}(SR) should increase with decreasing T (or L). These features are in fact observed in the experimental data for vacancy pit diffusion on Ag(111).[13]

Vacancy pit diffusion on Ag(111). Here, one finds that $E_e \approx 0.28-0.31$ eV is large, $\delta_{KES} \approx 0.05$ eV is small,[11,30] and $\phi \approx 0.19$ eV as in Sec. III. Thus, one estimates that $E_{eff}(SR) \approx 0.52-0.55$ eV (continuum) and $E_{eff}(SR) \approx 0.7$ eV (faceted). The former value is reasonably consistent with experimental results for vacancy pit diffusion of $E_{eff}(SR) \approx 0.5$ eV for larger L.[2,13] However, as noted in Sec. III, the experimentally observed $\beta \approx 1.5$ deviates significantly below the continuum value. Correspondingly, the experimentally observed $E_{eff}(SR) \approx 0.6$ eV for small pit sizes is somewhat above the continuum theory value, but below the completely faceted value.

Vacancy pit diffusion on Ag(100). Here, one has that $E_e = 0.25$ eV based on DFT analysis.[31] We estimate that $\delta_{KES} \approx 0.16$ eV,(Ref. 21, 26, and 27) and $\phi \approx 0.21$ eV from Sec. III. Thus, it follows that $E_{eff}(SR) \approx 0.62$ eV (continuum) and $E_{eff}(SR) \approx 0.8$ eV (faceted). Unfortunately, there has been no previous experimental determination of $E_{eff}(SR)$ for adatom island or vacancy pit diffusion. However, related studies of periphery-diffusion-mediated relaxation of step-edge nanostructures[25] suggest values in this range. For example, we have estimated that the initial rate of decay of the height of a 10×10 atom square protrusion on a close packed step edge equals 7 a/s at 300 K (Ref. 25) versus 0.14 a/s at 260 K (Ref. 32) This corresponds to a value of $E_{eff}(SR) \approx 0.67 \pm 0.1$ eV although we caution that there is considerable uncertainty in our estimates of decay rates. As noted in Sec. III, the experimentally observed value of $\beta \approx 2.3$ for adatom islands is below the continuum value. We assume that this value $\beta \approx 2.3$ also applies for vacancy pits and consequently expect that $E_{eff}(SR)$ should be somewhat above the value predicted from continuum theory.

V. ANALYSIS OF SMOLUCHOWSKI VERSUS OSTWALD RIPENING RATES

Integrating all of the results for energetics from Secs. III and IV to determine appropriate effective energy barriers for ripening (as summarized in Table I), we now provide a comparison of rates for SR and OR of vacancy pits for Ag(111) and Ag(100).

Vacancy pit ripening on Ag(111). We compare the rates (2) for SR and OR (=ORA here):

$$K_{SR} \approx \nu_{SR} \exp[-0.56/(k_B T)](L_{av})^{-2.5}$$

versus

$$K_{ORA} \approx \nu_{ORA} \exp[-0.80/(k_B T)](L_{av})^{-1}, \quad (6)$$

in units of s^{-1} with $k_B T$ in eV. For SR, we have used $\beta = 1.5$ (so $m=2.5$) and $E_{eff}=0.56$ eV which is somewhat above the value of E_{eff}(SR) from continuum theory. For ORA, adatom mass transport is inhibited by a step-edge barrier $\delta_{ES} \approx 0.13$ eV, with an associated characteristic Ehrlich-Schwoebel length $L_{ES}=\exp[\delta_{ES}/(k_B T)]-1 \approx 152$ at 300 K. Since L_{ES} is somewhat above the typical pit separation of ~ 100, we have used the attachment-detachment-limited exponent $m=1$ (although the effective value could be somewhat higher). See Appendix A. For a quantitative comparison, it remains to assess the prefactors. Based on analysis of experimental data in Appendix C, we assign $\nu_{SR} \approx 10^{11.1}$ s^{-1} and $\nu_{ORA} \approx 10^{11.3}$ s^{-1}, so that $K_{SR} \approx 47(L_{av})^{-2.5}$ versus $K_{ORA} \approx 0.007(L_{av})^{-1}$ at 300 K. This implies that SR should dominate OR below a crossover size of $L_{SR \to OR} \approx 350$. See Fig. 3(a). Thus, for the experimental size range $L_{av} \approx 30-50$, it follows that SR should completely dominate at 300 K (as observed). For higher temperatures around 350 K, the crossover size decreases to $L_{SR \to OR} \approx 94$ and the typical experimental L_{av} is larger than at 300 K, so OR should become competitive with SR.

Vacancy pit ripening on Ag(100). We compare the rates (2) for SR and OR (=ORV here):

$$K_{SR} \approx \nu_{SR} \exp[-0.65/(k_B T)](L_{av})^{-3.3}$$

versus

$$K_{ORV} \approx \nu_{ORV} \exp[-0.80/(k_B T)](L_{av})^{-2}, \quad (7)$$

in units of s^{-1} with $k_B T$ in eV. For SR, we have used $\beta = 2.3$ and $E_{eff}=0.65$ eV, somewhat above the prediction of continuum theory. This choice of β is based on the assumption that vacancy pits and adatom islands of the same size have similar diffusion coefficients. Some experimental data supporting this claim were provided in Sec. II. In addition, we have run simulations of the atomistic model for periphery-diffusion-mediated cluster diffusion described in Ref. 27. Results from these simulations at 300 K choosing $\phi=0.2$ and $\delta_{KES}=0$ support this claim for sizes above L

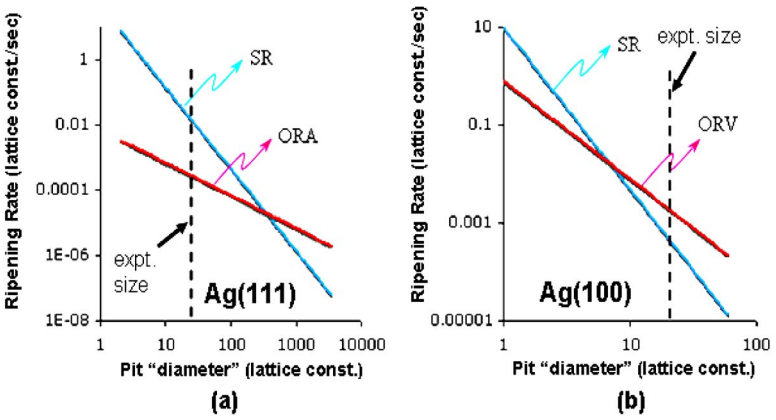

FIG. 3. (Color online) Crossover from SR to OR in coarsening rates K with increasing linear pit size L at 300 K for (a) Ag(111) and (b) Ag(100). The dashed vertical lines denote typical experimental sizes.

$=30$ (cf. $L_c \approx 70$). The pit diffusion coefficient is somewhat lower than the island diffusion coefficient for smaller sizes, but this could reflect limitations of our treatment of periphery diffusion (which is likely too inhibited for concave step-edge geometries characteristic of pits). For OR=ORV, we have used that ORV is terrace-diffusion-limited, resulting in a scaling exponent $m=2$. Based on analysis of experimental data in Appendix C, we assign $\nu_{SR} \approx 10^{12}\ s^{-1}$ and $\nu_{ORV} \approx 10^{13.3}\ s^{-1}$, so that $K_{SR} \approx 10(L_{av})^{-3.3}$ versus $K_{ORV} \approx 0.8(L_{av})^{-2}$ at 300 K. This implies that OR should dominate SR above a crossover size of $L_{SR \to OR} \approx 7$. See Fig. 3(b). Thus, for the experimental size range, $L_{av} \approx 35$, it follows that OR should dominate at 300 K (as observed). For lower temperatures around 275 K, the crossover size increases to $L_{SR \to OR} \approx 22$ and the typical experimental L_{av} is smaller than at 300 K, so SR should become competitive with OR (although both processes are very slow at this temperature).

We caution that there are significant uncertainties in the above analyses. Fairly small changes in effective energies produce significant changes in the rates. Also, there is considerable uncertainty in prefactors, and these also have an effect on the rates. However, we believe that the above analysis of ripening rates and their crossover with vacancy pit size captures the essential features of ripening on Ag surfaces.

VI. CONCLUSIONS

The distinct ripening behavior for vacancy pits on Ag(111) versus Ag(100) surfaces has been elucidated in terms of the underlying atomistic mass transport pathways, the energetics of those pathways, and the scaling of the ripening rate with pit size. OR of vacancy pits on Ag(111) is inoperative primarily due to a large effective barrier. This large barrier derives in part from the presence of a large Ehrlich-Schwoebel step-edge barrier if one considers mass transport via single adatoms or from a high terrace diffusion barrier if one considers mass transport via single-vacancy diffusion. OR of vacancy pits is operative on Ag(100) where mass transport is dominated by single-vacancy diffusion in part due to its lower terrace diffusion barrier (relative to that for single adatoms). SR is also inhibited relative to OR for Ag(100) due to the relatively large size of the pits. The type of analysis presented above can be extended to compare ripening mechanisms for vacancy pits on Cu(100) and Cu(111) surfaces.[3]

The above approach is also effective in elucidating the different ripening mechanisms observed for adatom islands at 300 K, either on Ag (Refs. 2 and 6) or Cu (Refs. 3 and 15) single-crystal surfaces. Interestingly, adatom islands ripen via ORA on Ag(111),[6] in contrast to SR for vacancy pits on Ag(111). For ORA of adatom islands (unlike pits), the step-edge barrier need not be surmounted during mass transport. Furthermore, adatom islands ripen via SR on Ag(100),[2] in contrast to OR for vacancy pits on Ag(100). OR is inhibited for islands relative to pits in part due to the higher diffusion barrier for adatoms of $E_d(\text{ad}) \approx 0.43$ eV compared to that for vacancies of $E_d(\text{vac}) \approx 0.35$ eV. Appendix D provides a more detailed analysis of OR versus SR pathways for adatom islands on Ag surfaces.

ACKNOWLEDGMENTS

M.S., J.M.W., C.J.J., P.A.T., and J.W.E. were supported for this work by NSF Grant No. CHE-0414378. D.J.L. was supported by the Division of Chemical Sciences, U.S. Department of Energy (DOE), BES. The work was performed at Ames Laboratory which is operated for the U.S. DOE by Iowa State University under Contract No. DE-AC02-07CH11358.

APPENDIX A: OR AND SR RIPENING KINETICS

For *Ostwald ripening*, analysis of kinetics is based on consideration of the evolution of a single pit or island of "diameter" $L=L(t)$ within a sea of other pits or islands which are described as an effective medium. Evolution is determined by solving a boundary value problem for the quasi-steady-state diffusion equation for mass transport across the surface with the appropriate boundary conditions. At the island or pit edge, one requires that the normal gradient of carrier density at the island edge is given by the ratio of the "excess density" at island edge to the attachment length, $L_{attach}=\exp[\delta/(k_BT)]-1$, where δ denotes any extra barrier for attachment. This excess density is the difference between the density on a terrace and the equilibrium Gibbs-Thomson density for the curved step edge (see Sec. III). When $\delta=0$, so $L_{attach}=0$, this boundary condition forces the terrace density

to equal the equilibrium density. Another boundary condition is imposed at a "large" distance from the island or pit which corresponds to the average island or pit separation $L_{\rm isl} \sim \varphi^{-1/2} L_{\rm av} \sim \varphi^{-1/2} L$, where φ denotes the areal coverage of the embedded phase. Specifically, one sets the carrier density to a constant corresponding to the equilibrium density at the edge of islands or pits with mean size $L_{\rm av}$. Solving this boundary value problem after linearizing the boundary conditions for small curvature of island or pit edges yields[1,4,33]

$$\frac{d}{dt}L \sim D\rho_0 \gamma L^{-1}[L_{\rm attach} + L\ln(\varphi^{-1/2})]^{-1}[L/L_{\rm av} - 1], \tag{A1}$$

where D is the terrace diffusion coefficient and ρ_0 and γ are defined in Sec. III. It follows that $dL/dt \sim -1/L$, as $L \to 0$, in the attachment-detachment-limited regime of large $L_{\rm attach}$ (so that pit or island area $A \sim L^2$ decays linearly), and $dL/dt \sim -1/L^2$, as $L \to 0$, in the terrace-diffusion-limited regime of small $L_{\rm attach}$ (so that areas decay non-linearly as mentioned in Sec. II).

Substitution of relation (A1) into the continuity equation for the pit or island size distribution and extraction of self-similar scaling solutions leads to time scaling for $L_{\rm av}$ of the form (1) with $n=1/2$ for attachment-detachment-limited ripening and $n=1/3$ for terrace-diffusion-limited ripening.[1,4,33] In our applications, $\delta=0$ and $L_{\rm attach}=0$ for terrace-diffusion-mediated intralayer transport, whereas $\delta=\delta_{\rm ES}$ and $L_{\rm attach}=L_{\rm ES}$ for attachment-detachment-limited interlayer transport of adatoms in the presence of a step-edge barrier.

For *Smoluchowski ripening* of vacancy pits, an analysis of the evolution of the mean linear pit size $L_{\rm av}$ is based on a simple rate equation analysis for the mean pit density $N_{\rm pit} \sim \varphi (L_{\rm av})^{-2}$ for areal coverage φ of islands or pits. It is expected that[7,9]

$$\frac{d}{dt}N_{\rm pit} \sim -D_{\rm pit}(L_{\rm av})(N_{\rm pit})^2 \sim -D_0 \exp[-E_{\rm eff}/(k_B T)] \times (N_{\rm pit})^{(4+\beta)/2}, \tag{A2}$$

which can be readily integrated to obtain time evolution of the form (1) for $L_{\rm av} \sim \varphi^{1/2}\ (N_{\rm pit})^{-1/2}$ with $n=1/(2+\beta)$. The treatment of SR kinetics for adatom islands is essentially identical.

APPENIDX B: DFT ANALYSIS OF ENERGETICS

Our DFT studies were performed using the Vienna *ab initio* simulation package (VASP).[34,35] We employ the generalized gradient approximation (GGA) with the Perdew-Burke-Ernzerhof (PBE) exchange-correlation functional[36] and the projector augmented wave (PAW) method.[37] We use the DFT theory equilibrium bulk lattice constant of 0.417 nm for fcc Ag. For the Ag(111) surface, calculations were performed on five-layer slabs of Ag substrate separated by ~1.2 nm of vacuum. For the Ag(100) surface, four-layer slabs of substrate separated by ~1.9 nm of vacuum were used. We checked for the effects of substrate atom relaxation. These effects are generally very small in calculations of adatom diffusion or NN adatom interactions, but are significant for vacancy diffusion. Results for diffusion barriers are presented in Table II and for NN adatom interactions in Table III. These tables also show the size of the lateral supercell used in the calculations, as well as the numbers of k points and thus the sensitivity of results on this choice. Of particular note is the slow convergence with increasing supercell size of the NN adatom interaction, ϕ, for the Ag(111) surface. See Ref. 38 for similar observations on slow convergence for a strained-layer heteroepitaxial system.

TABLE II. DFT estimates of terrace diffusion barriers for isolated adatoms and vacancies.

Surface	Species	Supercell size	k points	E_d (eV)
Ag(100)	Adatom	2×2	(4 4 1)	0.433
			(6 6 1)	0.429
Ag(100)	Vacancy	3×3	(2 2 1)	0.328
			(4 4 1)	0.376
			(6 6 1)	0.351
Ag(111)	Adatom	2×2	(10 10 1)	0.010
Ag(111)	Vacancy	3×3	(4 4 1)	0.485
			(6 6 1)	0.580

APPENDIX C: PREFACTOR DETERMINATION FOR SCALING RELATIONS

For quantitative comparison of *Ostwald ripening* (ORA or ORV) and *Smoluchowski ripening* (SR) rates, it is necessary to assess the prefactors in (2). This is achieved here by matching the experimentally observed rates for ripening with the scaling forms (2).

For *ORA of pits on Ag(111)*, one might expect that the prefactor is not readily assessed since SR dominates in this system. However, attachment-detachment-limited decay of single vacancy pits has been observed for special geometries at 300 K.[1,39] Consequently, one can exploit the feature that

TABLE III. DFT estimates of NN adatom interaction energies ϕ. To determine ϕ, a single NN pair of adatoms is placed within each supercell. Note that for the smallest 2×2 supercell, the adatoms form a linear chain, so one must account for two NN interactions per supercell. In all other cases, there is a single isolated NN pair of adatoms within each supercell.

Surface	Supercell size	k points	ϕ (eV)
Ag(100)	2×2	(10 10 1)	0.226
	3×3	(10 10 1)	0.216
	4×4	(10 10 1)	0.183
Ag(111)	2×2	(12 12 1)	0.233
	3×3	(6 6 1)	0.153
	4×4	(4 4 1)	0.229
	5×5	(4 4 1)	0.200
	6×6	(2 2 1)	0.196

the observed (constant) rate of decay to zero of pit area A equals 3.6 times the (constant) rate of increase of the mean pit area A_{av} for attachment-detachment-limited OR of an array of pits.[40] Using that $dA/dt \approx -0.04$ site/s from Refs. 1 and 39, we obtain that $dA_{av}/dt \approx 0.011$ site/s at 300 K. Since $A_{av} \approx \pi/4(L_{av})^2$, it follows that

$$K_{ORA} = dL_{av}/dt \approx 0.007(L_{av})^{-1} \text{ at } 300 \text{ K}. \quad \text{(C1)}$$

Then, using $E_{eff}=0.8$ eV yields a prefactor in (2) equal to $\nu=\nu_{ORA} \approx 10^{11.3}$ s^{-1} for Ag(111).

For *ORV of pits on Ag(100)*, our data at 300 K with $\varphi \approx 0.2$ ML indicate that the pit density decreases from an initial value of $N_{pit} \approx 1.2 \times 10^{-4}$/site to $N_{pit} \approx 0.76 \times 10^{-4}$/site after 6 h. Using

$$N_{pit} \approx \varphi(L_{av})^{-2} \approx N_0(1 + t/\tau)^{-2/3} \quad \text{(C2)}$$

for terrace-diffusion-limited ORV, consistent with (1), yields $\tau \approx 27130$ s, and

$$K_{ORV} = dL_{av}/dt \approx 0.8(L_{av})^{-2} \text{ at } 300 \text{ K}. \quad \text{(C3)}$$

Using $E_{eff} \approx 0.8$ eV then yields a prefactor in (2) of $\nu = \nu_{ORV} \approx 10^{13.3}$ s^{-1} for Ag(100).

For *SR of pits on Ag(111)* at 300 K, using the data in Ref. 5 with $\varphi \approx 0.15$ ML, the pit density decreases from an initial value of $N_{pit} \approx 1.0 \times 10^{-4}$/site to $N_{pit} \approx 0.67 \times 10^{-4}$/site after 61 min. Using

$$N_{pit} = \varphi(A_{av})^{-1} \approx 4\pi^{-1}\varphi(L_{av})^{-2} \approx N_0(1 + t/\tau)^{-0.57} \quad \text{(C4)}$$

with $\beta \approx 1.5$ yields $\tau \approx 3090$ s and

$$K_{SR} = dL_{av}/dt \approx 47(L_{av})^{-2.5} \text{ at } 300 \text{ K}. \quad \text{(C5)}$$

Then, using $E_{eff} \approx 0.56$ eV yields a prefactor in (2) of $\nu = \nu_{SR} \approx 10^{11.1}$ s^{-1} for Ag(111).

For *SR of pits on Ag(100)* surface at 300 K, we assume the same kinetics for vacancy pits and adatom islands. Then, we can use the result from Ref. 14 that $L_{av}/L_0 \approx 1.93$ for $t = 1667$ s together with $\beta \approx 2.3$ to obtain from (1) an estimate of $\tau \approx 6410$ s and

$$K_{SR} = dL_{av}/dt \approx 2(L_{av})^{-3.3} \text{ at } 300 \text{ K}. \quad \text{(C6)}$$

Then, using $E_{eff} \approx 0.65$ eV yields a prefactor in (2) of $\nu = \nu_{SR} \approx 10^{11.3}$ s^{-1}. An alternative strategy exploits our result for $D_{pit}(L \approx 25) = 3.5 \times 10^{-3}$ a^2/s at 300 K, together with $\beta \approx 2.3$ and $E_{eff} \approx 0.65$ eV to estimate that $D_0 \approx 10^{11.5}$ a^2/s. A refined analysis based on Eq. (A2) but incorporating appropriate φ dependence[7] indicates that

$$\nu = \nu_{SR} \approx (2 + \beta)4\varphi(1 - \varphi^{1/2})^{-2}D_0$$
$$\approx 10^{12.5}/\text{s for } \varphi \approx 0.2 \text{ ML}. \quad \text{(C7)}$$

Thus, we choose $\nu = \nu_{SR} \approx 10^{12}$ s^{-1} for vacancy pit ripening on Ag(100).

APPENDIX D: OR vs SR FOR ADATOM ISLANDS

For *adatom islands on Ag(111)*, OR occurs via adatom transport (ORA) given the far lower terrace diffusion barrier for adatoms compared with vacancies and noting that no step-edge barrier need be surmounted. Our estimate of the effective barrier $E_{eff}(OR) = E_d(ad) + 3\phi \approx 0.67$ eV is quite close to the experimental estimate of 0.71 eV.[39] Note that this effective energy is significantly lower than the value 0.8 eV for ORA of vacancy pits. ORA of adatom islands is terrace-diffusion-limited so that one has that

$$K_{ORA} = \nu_{ORA} \exp[-0.67/(k_BT)](L_{av})^{-2}. \quad \text{(D1)}$$

Analysis of the ripening data in Ref. 2 indicates that $\nu_{ORA} \approx 10^{12.3}$ s^{-1}, so that $K_{ORA} \approx 12(L_{av})^{-2}$ at 300 K.

Characterization of the kinetics of SR of adatom islands on Ag(111) is more difficult as this process is not observed experimentally at 300 K. However, adatom islands are mobile and their diffusivity has been characterized.[13] The effective activation barrier was estimated as $E_{eff}(SR) \approx 0.53$ eV,[13] quite close to the experimental estimates for vacancy pits and consistent with continuum theory estimate (for either pits or islands) of 0.54 eV. The experimental estimate for the size scaling exponent of $\beta \approx 1.6$ (Ref. 13) is also close to that for vacancy pits. Thus, one concludes that the diffusivity of islands and pits of the same size on Ag(111) is quite similar. Then, we can adopt the expression for K_{SR} for pits in (6) to describe SR of islands. In this case, using Eq. (D1), one finds a crossover from SR of adatom islands to ORA as the typical size increases above $L_{SR \to OR} \approx 10$. This is consistent with experimental observations of OR as typical island sizes in Refs. 2 and 5 exceed this crossover value.

For *adatom islands on Ag(100)*, SR dominates coarsening at 300 K. Estimation of the effective barrier yields $E_{eff}(SR) = E_e + \phi + \delta_{KES} \approx 0.65$ eV (continuum), as for vacancy pits. Utilizing the size scaling exponent for adatom island diffusion of $\beta \approx 2.3$, one has

$$K_{SR} = \nu_{SR} \exp[-0.65/(k_BT)](L_{av})^{-3.3}. \quad \text{(D2)}$$

Analysis of ripening data in Ref. 15 indicates that $\nu_{SR} \approx 10^{11.2}$ s^{-1}, so that $K_{SR} \approx 2.2(L_{av})^{-3.3}$ at 300 K.

Characterization of the kinetics of OR of adatom islands on Ag(100) by adatom transport (ORA) is more difficult. The effective activation barrier can be estimated from $E_{eff}(ORA) = E_d(ad) + 2\phi \approx 0.85$ eV. The prefactor of the ripening rate is not known, but adopting a similar value to that for OR of vacancy pits on Ag(100) yields $K_{ORA} \approx 10^{13} \exp[-0.85/(k_BT)](L_{av})^{-2}$. This in turn implies a crossover from SR to ORA when the typical island size exceeds $L_{SR \to OR} \approx 18$, a value above typical experimental sizes in Ref. 6.

Surprisingly, for adatom islands on metal (100) surfaces, one should not discount the possibility of OR by vacancy transport (ORV). The lower terrace diffusion barrier for vacancies compared with adatoms can compensate for any inhibition due to the required interlayer transport. For Ag(100), the effective barrier for ORV is $E_{eff}(ORV) = E_d(vac) + 2\phi + \delta_{ESV} \approx 0.75 + \delta_{ESV}$, where δ_{ESV} denotes any additional barrier for interlayer transport of vacancies. If δ_{ESV} is below 0.1 eV, then ORV has an energetic advantage over ORA. Note that while ripening of adatom islands on Cu(100) occurs via SR at 300 K, ORV dominates at around 340 K.[41,42]

*Current address: Komag Inc., 1710 Automaton Parkway, San Jose, CA 95121, USA.

[1] L. Ratke and P. W. Voorhees, *Growth and Coarsening* (Springer, Berlin, 2001).
[2] K. Morgenstern, Phys. Status Solidi B **242**, 773 (2005).
[3] M. Giesen, Prog. Surf. Sci. **68**, 1 (2001).
[4] M. Zinke-Allmang, L. C. Feldman, and M. H. Grabow, Surf. Sci. Rep. **16**, 377 (1992).
[5] G. Rosenfeld, K. Morgenstern, M. Esser, and G. Comsa, Appl. Phys. A: Mater. Sci. Process. **69**, 489 (1999).
[6] J.-M. Wen, J. W. Evans, M. C. Bartelt, J. W. Burnett, and P. A. Thiel, Phys. Rev. Lett. **76**, 652 (1996).
[7] C. R. Stoldt, C. J. Jenks, P. A. Thiel, A. M. Cadilhe, and J. W. Evans, J. Chem. Phys. **111**, 5157 (1999).
[8] S. V. Khare, N. C. Bartelt, and T. L. Einstein, Phys. Rev. Lett. **75**, 2148 (1995).
[9] P. Meakin, Physica A **165**, 1 (1980).
[10] J.-M. Wen, S.-L. Chang, J. W. Burnett, J. W. Evans, and P. A. Thiel, Phys. Rev. Lett. **73**, 2591 (1994).
[11] E. Cox, M. Li, P.-W. Chung, C. Ghosh, T. S. Rahman, C. J. Jenks, J. W. Evans, and P. A. Thiel, Phys. Rev. B **71**, 115414 (2005).
[12] K. Morgenstern, G. Rosenfeld, B. Poelsema, and G. Comsa, Phys. Rev. Lett. **74**, 2058 (1995).
[13] D. C. Schlosser, K. Morgenstern, L. K. Verheij, G. Rosenfeld, F. Besenbacher, and G. Comsa, Surf. Sci. **465**, 19 (2000).
[14] K. Morgenstern, G. Rosenfeld, and G. Comsa, Phys. Rev. Lett. **76**, 2113 (1996).
[15] W. W. Pai, A. K. Swan, Z. Zhang, and J. F. Wendelken, Phys. Rev. Lett. **79**, 3210 (1997).
[16] By virtue of Wulff's construction for equilibrium island or pit shapes, the ratio of local step energy to the local pedal radius, γ/R, equals the product of the local step stiffness and the local curvature, $\tilde{\gamma}\kappa$. Both quantities are constant along the step edge. See W. K. Burton, N. Cabrera, and F. C. Frank, Proc. R. Soc. London, Ser. A **243**, 40 (1951).
[17] J. W. Evans, P. A. Thiel, and M. C. Bartelt, Surf. Sci. Rep. **61**, 1 (2006).
[18] K. A. Fichthorn and M. Scheffler, Phys. Rev. Lett. **84**, 5371 (2000).
[19] P. Stoltze, J. Phys.: Condens. Matter **6**, 9495 (1994).
[20] P. A. Thiel and J. W. Evans, J. Phys. Chem. B **108**, 14428 (2004).
[21] K. J. Caspersen, A. R. Layson, C. R. Stoldt, V. Fournee, P. A. Thiel, and J. W. Evans, Phys. Rev. B **65**, 193407 (2002).
[22] P. Feibelman (unpublished).
[23] H. Mehl, O. Biham, I. Furman, and M. Karimi, Phys. Rev. B **60**, 2106 (1999).
[24] N. Quaas, M. Wenderoth, and R. G. Ulbrich, Surf. Sci. **550**, 57 (2004).
[25] C. R. Stoldt, A. M. Cadilhe, C. J. Jenks, J.-M. Wen, J. W. Evans, and P. A. Thiel., Phys. Rev. Lett. **81**, 2950 (1998).
[26] W. W. Pai, J. F. Wendelken, C. R. Stoldt, P. A. Thiel, J. W. Evans, and D.-J. Liu, Phys. Rev. Lett. **86**, 3088 (2001).
[27] D.-J. Liu and J. W. Evans, Phys. Rev. B **66**, 165407 (2002).
[28] P. Jensen, N. Combe, H. Larralde, J. L. Barratt, C. Misbah, and A. Pimpinelli, Eur. Phys. J. B **11**, 497 (1999).
[29] G. Mills, T. R. Mattsson, L. Mollnitz, and H. Metiu, J. Chem. Phys. **111**, 8639 (1999).
[30] H. Brune, H. Roder, K. Bromann, K. Kern, J. Jacobsen, P. Stoltze, K. Jacobsen, and J. K. Norskov, Surf. Sci. **349**, L115 (1996).
[31] B. D. Yu and M. Scheffler, Phys. Rev. B **55**, 13916 (1997).
[32] C. R. Stoldt, Ph.D. thesis, Iowa State University, 1999.
[33] F. Hausser and A. Voigt, Phys. Rev. B **72**, 035437 (2005).
[34] G. Kresse and J. Hafner, Phys. Rev. B **47**, R558 (1993).
[35] G. Kresse and J. Furthmüller, Phys. Rev. B **54**, 11169 (1996).
[36] J. P. Perdew, K. Burke, and M. Ernzerhof, Phys. Rev. Lett. **77**, 3865 (1996).
[37] G. Kresse and D. Joubert, Phys. Rev. B **59**, 1758 (1999).
[38] W. Luo and K. A. Fichthorn, Phys. Rev. B **72**, 115433 (2005).
[39] K. Morgenstern, G. Rosenfeld, E. Laegsgaard, F. Besenbacher, and G. Comsa, Phys. Rev. Lett. **80**, 556 (1998).
[40] N. C. Bartelt, W. Theis, and R. M. Tromp, Phys. Rev. B **54**, 11741 (1996).
[41] J. B. Hannon, C. Klunker, M. Giesen, H. Ibach, N. C. Bartelt, and J. C. Hamilton, Phys. Rev. Lett. **79**, 2506 (1997).
[42] C. Klunker, J. B. Hannon, M. Giesen, H. Ibach, G. Boisvert, and L. J. Lewis, Phys. Rev. B **58**, R7556 (1998).